Master thesis
A Study of the Lorentz Angle for JLC CDC

Tokyo University of Agriculture and Technology
Kotoyo Hoshina

March 17, 1999

Abstract

We have established a Lorentz angle measurement system. The Lorentz angle is measured for the different proportion of CO_2 and Isobutane gas mixtures (95:5), (90:10), and (85:15) as a function of electric fields ($0.4 \sim 2.0$ kV/cm) at the different magnetic fields ($0 \sim 1.5$ T). The results of the measurements are compared with the prediction of calculations using the gaseous detectors simulation program GARFIELD. there are small systematic disagreements between calculations and measurements which are more significant at the high magnetic fields. In order to explain these disagreements we need more detailed study of simulation program GARFIELD and more precise experimental data.

Also we propose a new Lorentz angle measurement system by using two simultaneous laser beams which will give us more accurate estimation of Lorentz angle especially at the higher magnetic fields.

Contents

1 Introduction **3**

2 Lorentz Angle and Single Cell Design **5**

3 Drift of Gaseous Electrons in Static E and B fields **7**

4 Experimental Setup **10**
4.1 Optical setup 10
4.2 Chamber 12
4.3 Magnet 14
4.4 Data Acquisition(DAQ) System 14

5 Experimental Procedure and Data Analysis **17**
5.1 Experimental Procedure 17
5.2 Charge Centroid Method 19
5.3 Correction of the Induced Charges on Each Cathode Pad . . . 20
5.4 Calibration 21

6 Experimental Results **23**
6.1 Electric-Field Dependence of the Lorentz Angle 23
6.2 Extrapolation of the Lorentz Angle to 2 T 23
6.3 Comparison with GARFIELD Simulations 28
6.4 Electric-Field Dependence of ψ 28

7 Discussion **31**

8 Proposals of the Next Experiment **34**
8.1 Two Simultaneous Parallelized Beam System 34
8.2 New DAQ System 37
8.3 Calibration 37

9 Conclusion **39**

List of Figures

2.1 A typical geometry of a JLC CDC single cell 5
2.2 Drift lines for CO_2-Isobutane(90:10) 6

4.1 Schematic view of the experimental setup 11
4.2 A sketch of the test chamber 12
4.3 A sectional drawing of the test chamber (x-view) 13
4.4 Cathode pad 14
4.5 USHIWAKA V-B graph 15
4.6 DAQ Block Diagram 16

5.1 Illustration of the Lorentz angle measurement 18
5.2 Induced charges on cathode pads 19
5.3 Calibration curves of center of gravity (pad 13-16) 21
5.4 x dependence of σ (pad13-16) 22

6.1 Electric-field dependence(90:10) 24
6.2 Electric-field dependence(95:5) 25
6.3 Electric-field dependence(85:15) 25
6.4 Lorentz angle extrapolated at 2.0T(90:10) 26
6.5 Lorentz angle extrapolated at 2.0T(95:5) 26
6.6 Lorentz angle extrapolated at 2.0T(85:15) 27
6.7 Comparison with GARFIELD simulations for CO_2-isobutane (90:10) 28
6.8 Drift velocity of CO_2-Isobutane 29
6.9 Electric-field dependence of psi(90:10) 30

7.1 Magnetic-field dependence of σ 31
7.2 Time dependence of the center of gravity 32

8.1 Optical setup for the new experiment 35
8.2 Setup of the Flash ADC 36
8.3 Calibration of two-beam system 37
8.4 Position resolutions of G 38

Chapter 1

Introduction

High energy physics has made a remarkable progress after invention of particle accelerators. It led to the striking development of theories of elementary particles and resulted in the Standard Model, consisting of three generations of leptons and quarks. The model describes practically all the experimental data we have at present. The model describes also another hypothetical particle named Higgs, However, we have not discovered the Higgs particle yet.

The JLC (Japan Linear Collider) project is the post-TRISTAN high energy physics program recommended by the High Energy Committee in 1986. [1] JLC is an e^+e^- collider to test the standard model and explore the physics beyond it in the (sub) TeV region.

One of the most important characteristic features of e^+e^- experiment in this energy region is that all physics processes can be recognized in terms of known fundamental particles (leptons, quarks, and gauge bosons). To make maximum use of this advantage, we have to design our detector so as to exclusively reconstruct all final-state particles except neutrinos. Reconstruction of W and Z via jet invariant masses is very important in order to use their large decay branching function into quarks. To improve the mass resolution of the W and Z, we rely primarily on the tracking information for charged particles, though, of course, neutral particles are only detectable by the calorimeter. In this scheme, a good track-cluster matching is essential to determine the event topology correctly.

One of the most important physics targets of JLC is to find and study the intermediate mass Higgs boson . For this purpose, the detector should be capable of confirming the narrow decay width.

Taking those requirements into account, we set the following design criteria:

1. jet invariant mass resolution comparable with the natural width of the

W and Z,

2. lepton pair recoil mass resolution for $e^+e^- \to ZH$ comparable with the mean energy spread of $\sim$ 200 MeV.

The first criterion necessitates reconstructions of individual tracks in each jet from the gauge boson decays, thereby demanding good two-track separation (better than 2 mm). On the other hand, the second criterion constrains momentum resolution to be as good as $\sigma_{p_T}/p_T \sim 10^{-4} \times p_T(GeV)$.

Those requirements led us to a large cylindrical drift chamber with small jet cells as a candidate central tracking device (CDC:Central Drift Chamber). Lorentz angle, which is the deflection angle of the drift direction of gaseous electrons in an electrostatic field due to an additional magnetostatic field, is one of the most important parameters to determine the cell design of such a chamber.

In this thesis we present results from Lorentz angle measurements for candidate gas mixtures of CO_2 and isobutane. The structure of the thesis is as follows. In chapter 2, we describe the current single cell structure of CDC and how it depends on the Lorentz angle. Chapter 3 explains underlying physics for drift of gaseous electrons in static **E** and **B** fields in order to clarify relevant parameters to determine the Lorentz angle. Chapter 4 shows the experimental setup for our Lorentz angle measurements. We used a UV Laser beam which ionizes gas molecules and a test chamber which is equipped with cathode pads to detect the arrival positions of drift electrons. Chapter 5 is the explanation of data analysis. We used the center of gravity Method to calculate the arrival positions of drift electrons. The calibration data are also shown in this chapter. Chapter 6 gives results. It contains all experimental data, the extrapolated value of the Lorentz angle at 2 T, comparison with GARFIELD simulation, and electric-field dependence of ψ. In chapter 7, possible sources of measurement errors at higher magnetic fields are discussed. Chapter 8 contained a proposal of a new experiment to improve the data at higher magnetic fields. Finally, chapter 9 concludes the thesis.

Chapter 2

Lorentz Angle and Single Cell Design

The current structure of the small jet type single cell is shown Fig.2.1 [2]. S1 to S5 are sense wires. F1** to F10** are field shaping wires whose potentials change linearly in this order from -0.5 kV to -4.6 kV, and left and right edge field wires are held at -4.6 kV. The wire diameter is 30 μm for sense wires and 125 μm for others.

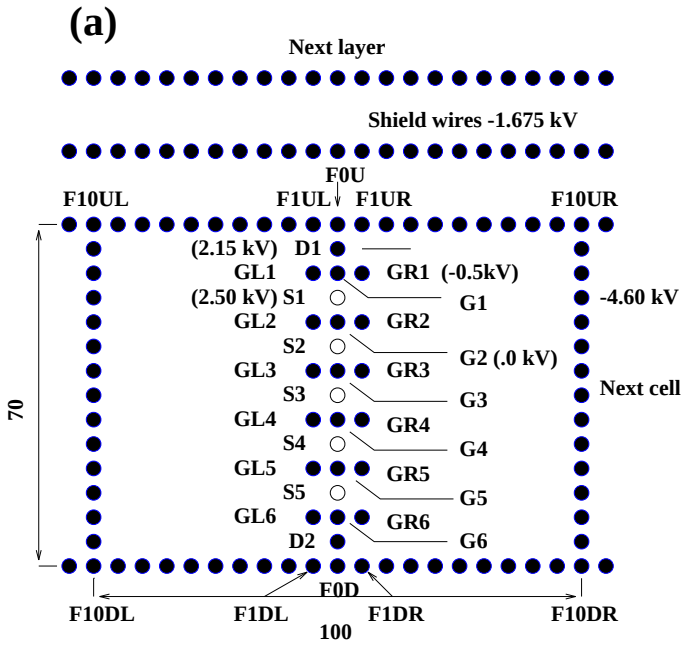

Figure 2.1: A typical geometry of a JLC CDC single cell

When a charged particle passes through the cell, the charged particle ionizes molecules of chamber gas along its track. After that, this primary

electrons drift toward sense wires. By measuring drift times of these electrons, we know where the charged particle has passed.

In order to decide its momentum from the curvature of the track, the CDC should be placed in a magnetic field. However, this magnetic field also bends drift lines of electrons. Fig.2.2 shows drift lines in our cell which were calculated with the GARFIELD program. The left picture gives drift lines without magnetic field. Those drift lines are parallel to the electric field. The right picture shows the drift lines at a magnetic field of 2 T. Those drift lines have a finite deflection angle to the electric field, and we call this angle the Lorentz angle. The Lorentz angle depends on electric and magnetic field, as well as gas mixture.

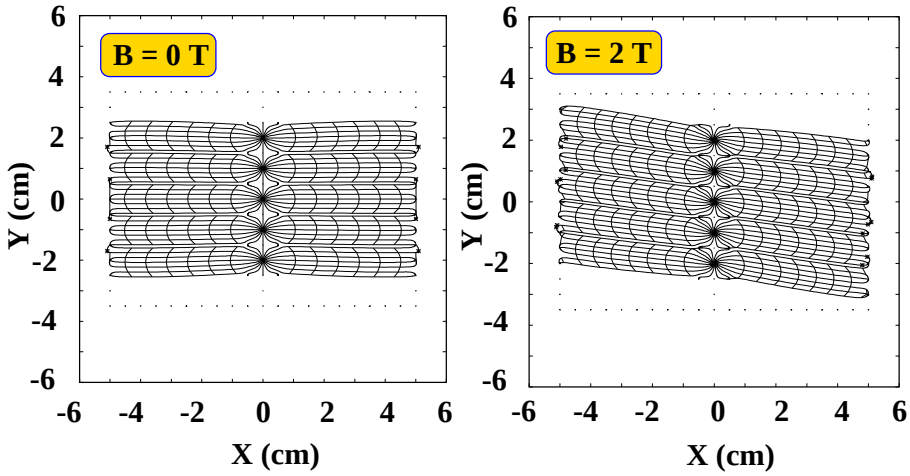

Figure 2.2: GARFIELD results of Drift lines (CO_2-Isobutane(90:10))

Fig.2.2 also shows acceptance of the Lorentz angle. When the Lorentz angle becomes exceedingly bigger, some drift electrons are absorbed by field wires before reaching a sense wire. Although we have a solution for this problem, to incline cells along with drift lines, we chose another solution to use a gas mixture which has small enough Lorentz angle to keep the original cell shape. It contributes to keep good two-track separation.

We chose CO_2-isobutane (90:10) gas mixture as a candidate of chamber gas. The purpose of the Lorentz angle measurement is to get the actual value of Lorentz angle for our gas mixture and to confirm the reliability of the GARFIELD simulation. In particular for this purpose, we consider that the error of the Lorentz angle should be below 10 % at the magnetic-field of 2 T.

Chapter 3

Drift of Gaseous Electrons in Static E and B fields

The main role of the central tracking device CDC is to measure the particle momentum. For this purpose, CDC must be placed in a high magnetic-field, high enough to bend high-energy particle tracks. However, the magnetic-field gives an influence to the drift of electrons. So, the mechanism of the electron drift in the magnetic-field must be studied in detail.

When an electric-field is applied across the drift region, the electrons produced by an ionizing particle drift along the electric-field direction if the magnetic-field is zero. If the magnetic-field is applied orthogonal to the electric-field, each drifting electron gets influence of a Lorentz force. We should start the discussion by writing down the most general expression for the drift velocity vector in the electric and magnetic-field [3].

The motion of charged particles under the influence of the electric and magnetic-field should be a helix movement with an angler velocity $\boldsymbol{\omega}$:

$$\boldsymbol{\omega} = -\frac{q\mathbf{B}}{m} \tag{3.0.1}$$

where $\mathbf{B}$ is the magnetic-field vector, m and q are the mass and electric charge of a charged particle. This helix movement can be divided into an orbital component and a parallel component, and the expressions of parallel component are:

$$\mathbf{v}_D = \mathbf{E} \times \frac{\mathbf{B}}{B^2} + \mathbf{v}_{\|} \tag{3.0.2}$$

$$m\dot{\mathbf{v}}_{\|} = q\mathbf{E}_{\|} \tag{3.0.3}$$

where $\mathbf{v}_D$ is the drift velocity vector of a charged particle, $\mathbf{E}$ is the electric-field vector, $\mathbf{v}_{\|}$ and $\mathbf{E}_{\|}$ are parallel components to $\mathbf{B}$. Those two equations (3.0.3), (3.0.3) derive $\mathbf{v}$ as following:

$$\mathbf{v} = \mathbf{v}_D + \boldsymbol{\omega} \times \mathbf{r}_b \tag{3.0.4}$$

where $\mathbf{r}_b$ is the position of electron in a plane of orthogonal to $\mathbf{v}_D$. Now, another force should be appended to equation (3.0.4). The electrons in gas collide frequently with molecules of gas. The Langevin Equation presents this effect as a function of time:

$$m\dot{\mathbf{v}} = q(\mathbf{E} + \mathbf{v} \times \mathbf{B}) + m\mathbf{A}(t) \tag{3.0.5}$$

where $m\mathbf{A}(t)$ describes a frictional force which is caused by the interaction of the particle with the gas. As well known, the drift velocity $\mathbf{v}_D$ doesn't depend on time, so that the time average of $\langle \mathbf{A}(t) \rangle$ have to cancel the acceleration of drift:

$$\langle \mathbf{A}(t) \rangle = -\frac{\mathbf{v}_D}{\tau} \tag{3.0.6}$$

where τ is the mean-time-interval of two collisions. The equation (3.0.5) is, therefore, written as following:

$$m\dot{\mathbf{v}}_D = \frac{q\mathbf{E}}{m} + \left(\mathbf{v}_D \times \frac{q\mathbf{B}}{m} \right) - \frac{\mathbf{v}_D}{\tau} \tag{3.0.7}$$

and when the electric-field is stable, $\dot{\mathbf{v}}_D$ should be equal to zero.

$$\frac{\mathbf{v}_D}{\tau} + \left(\frac{q\mathbf{B}}{m} \times \mathbf{v}_D \right) = \frac{q\mathbf{E}}{m} \tag{3.0.8}$$

Finally, $\mathbf{v}_D$ can be derived by equation (3.0.8).

$$\mathbf{v}_D = \frac{\mu}{1 + \omega^2\tau^2} \left(\mathbf{E} + \frac{\mathbf{E} \times \mathbf{B}}{B}\omega\tau + \frac{(\mathbf{E} \cdot \mathbf{B}) \cdot \mathbf{B}}{B^2}\omega^2\tau^2 \right) \tag{3.0.9}$$

where μ is the mobility of the electron:

$$\mu = \frac{q\tau}{m} \tag{3.0.10}$$

This drift velocity (3.0.9) has three components. One is parallel to $\mathbf{E}$, another is parallel to $\mathbf{B}$, and the last is orthogonal to $\mathbf{E}$ and $\mathbf{B}$. When $\omega\tau = 0$, little magnetic-field or little time interval from a collision to another collision, $\mathbf{v}_D$ indicates parallel to $\mathbf{E}$. On the other hand, when $\omega\tau \gg 1$, $\mathbf{v}_D$ points the direction of $\mathbf{B}$. If the magnetic-field takes a stable value, the ω should become a constant by equation (3.0.1), therefore, which direction is chosen for $\mathbf{v}_D$ depends on only mean-time-interval τ – the value decided by collisional cross section.

When the magnetic-field and electric-field are orthogonally crossed, the last term of equation (3.0.9) equal to 0. Thus, at $\mathbf{E} = (E_x, 0, 0)$ and $\mathbf{B} = (0, 0, B_Z)$, the components of $\mathbf{v}_D$ is:

$$\begin{aligned} v_x &= \mu E_x \frac{1}{1+\omega^2\tau^2} \\ v_y &= -\mu E_x \frac{\omega\tau}{1+\omega^2\tau^2} \\ v_z &= 0 \end{aligned} \tag{3.0.11}$$

the equation (3.0.11) shows that $\mathbf{v}_D$ lies on the (x, y) plane. That means, the electrons drift in the plane of orthogonal to $\mathbf{B}$ with a drift velocity as following:

$$|\mathbf{v}_D| = \sqrt{v_x^2 + v_y^2} = \mu E_x \frac{1}{\sqrt{1+\omega^2\tau^2}} \tag{3.0.12}$$

and the angle between $\mathbf{v}_D$ and $\mathbf{E}$ is given by equation as α(3.0.11).

$$\tan\alpha = \left|\frac{v_y}{v_x}\right| = \omega\tau \tag{3.0.13}$$

The α is called as a Lorentz Angle. From equation 3.0.1, ω depends on the magnetic field. On the other hand, τ has a relation with the electric field. Thus, in practically, the Lorentz angle can be expressed as a function of $\mathbf{E}$, $\mathbf{B}$, and $\mathbf{v}_{D0}$. Usually, we use the following equation instead of the equation (3.0.13): [4]

$$\tan\alpha = \psi \frac{B}{E} v_{D0} \tag{3.0.14}$$

where the dimensionless factor ψ is called a magnetic deflection coefficient which depends on the electric-field and the gas property.

Chapter 4

Experimental Setup

A schematic view of the setup for the Lorentz angle measurement is shown in Fig.4.1. In order to induce ionization in the drift chamber, a UV laser beam was used because of following advantages:

- Easiness of the position control
- No deflection of the laser beam in the magnetic-field
- Good reproducibility

Those advantages enabled the fast and precise data taking.

4.1 Optical setup

A Nd-YAG laser (frequency-quadrupled, wavelength 266 nm) produces pulses which has about 50 mJ maximum energy and about 5 nsec beam width with a frequency of 10 Hz. Then, the beam passes through a lens with focal length of 3000 mm. The reason why such a long-focus lens was used is to avoid a big change of the beam cross section in the chamber. In order to avoid the saturation of the pre-amp, the beam intensity is attenuated by using the surface reflection of a prism which reduces the beam intensity to 3 %. Then, the beam is reflected by 2 mirrors which are fixed on 2 micrometer stages. The first micrometer stage moves 2 mirrors and another micrometer stage along to the x-axis. The second mirror stage moves upper mirror along the y-axis in order to provide variable drift distance. This y-axis motion is converted to the z-axis (the direction of drift line) motion at inside of the chamber(see Fig.4.3.).

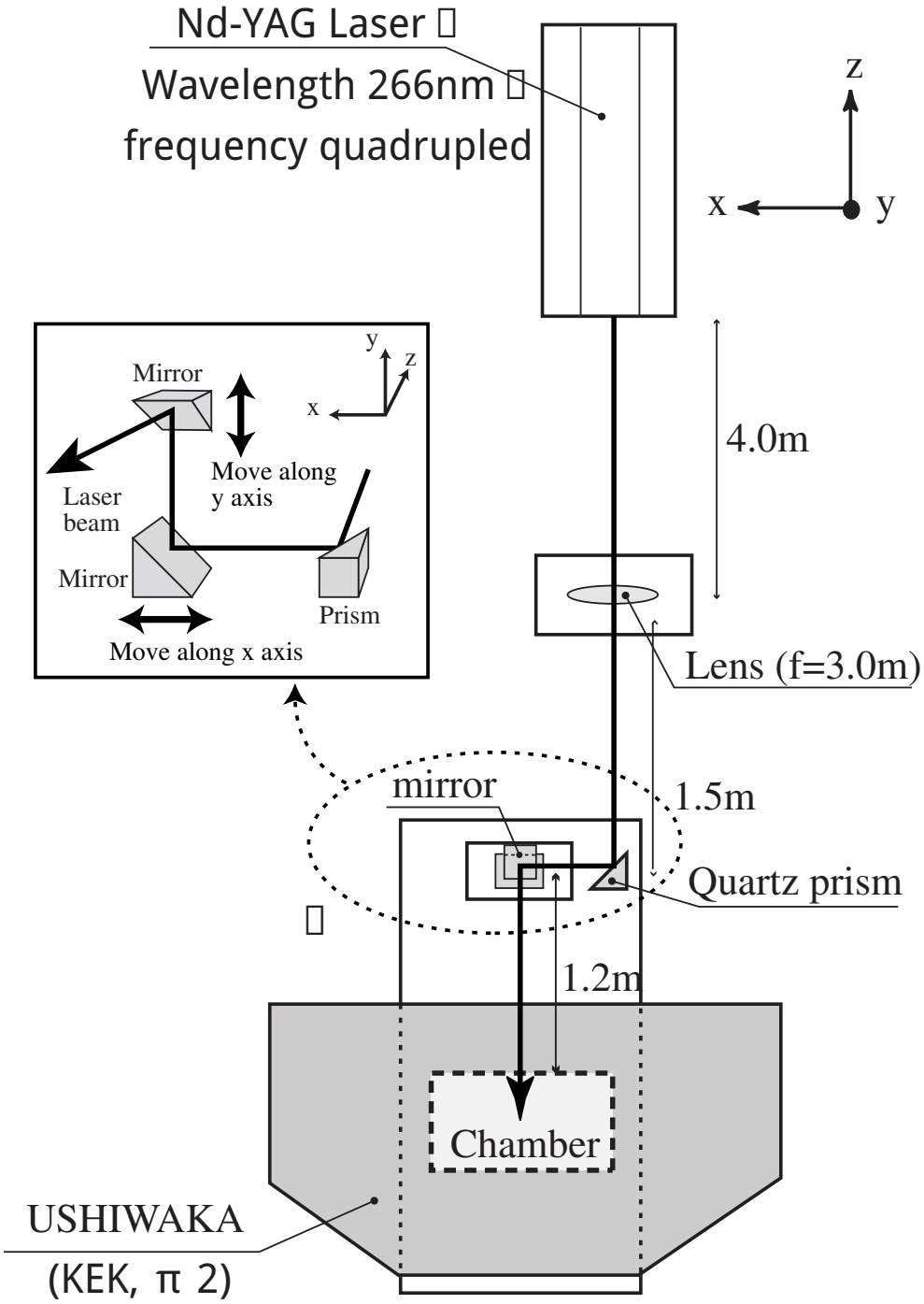

Figure 4.1: Schematic view of the experimental setup

4.2 Chamber

The test chamber is depicted in Fig.4.2 and Fig.4.3 [5]. It consists of 2 mirrors (45 degrees inclined) and 5 pre-amps and an aluminum box with 2 quartz windows which allow penetration of laser beam. The upper mirror converts beam incidental direction from the z-axis to the y-axis. The down one converts the beam direction from z-axis to y-axis, to avoid the reflected beam going back to the chamber. Pre-amp card has 32 channels, and one of the 5 pre-amp cards is for the anode signal, others are for cathode signals. The aluminum box has also 2 flexible hoses to provide the CO_2-Isobutane mixture at a rate of 100 ml/min. There are three parts inside the box, named Drift part, Gain part, and Cathode part.

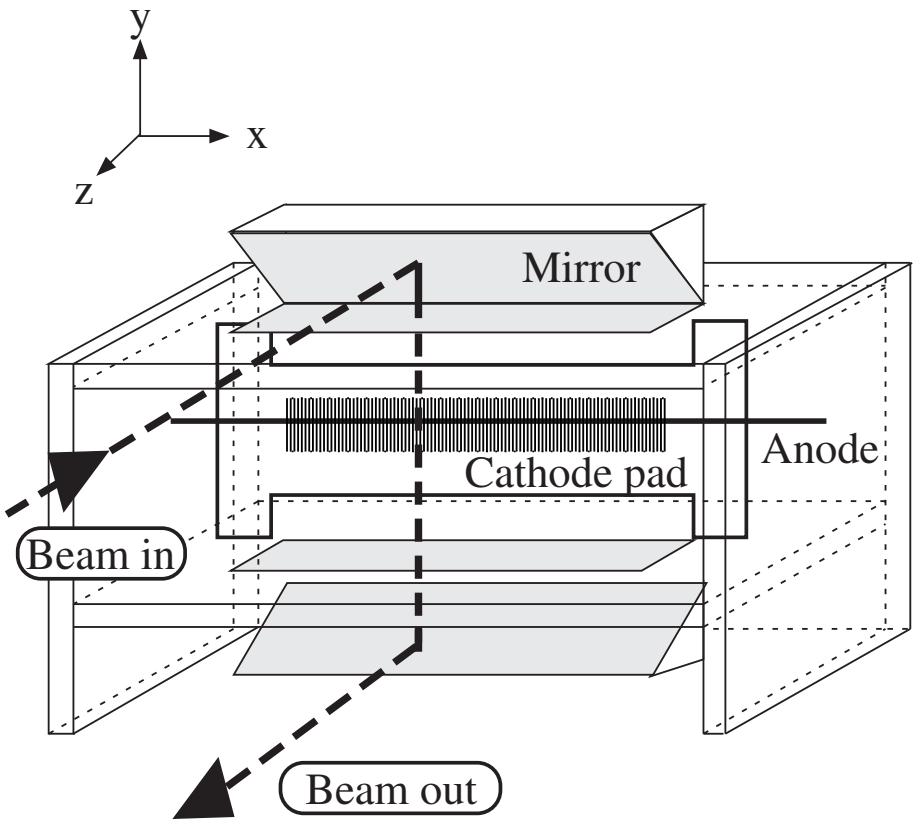

Figure 4.2: A sketch of test chamber

The Drift part consists of 10 pieces of copper plates (30×170 cm^2, 1.0 mm thick) which are arranged with a 5 mm space and connected each other by the 2.2 MΩ register. A homogeneous electric-field is generated by them. The negative high voltage is applied on the first plate, which has no window. The plates from the second to the tenth have a 20×150 cm^2 window at the center of the plate, and which allows electrons to pass through. The last

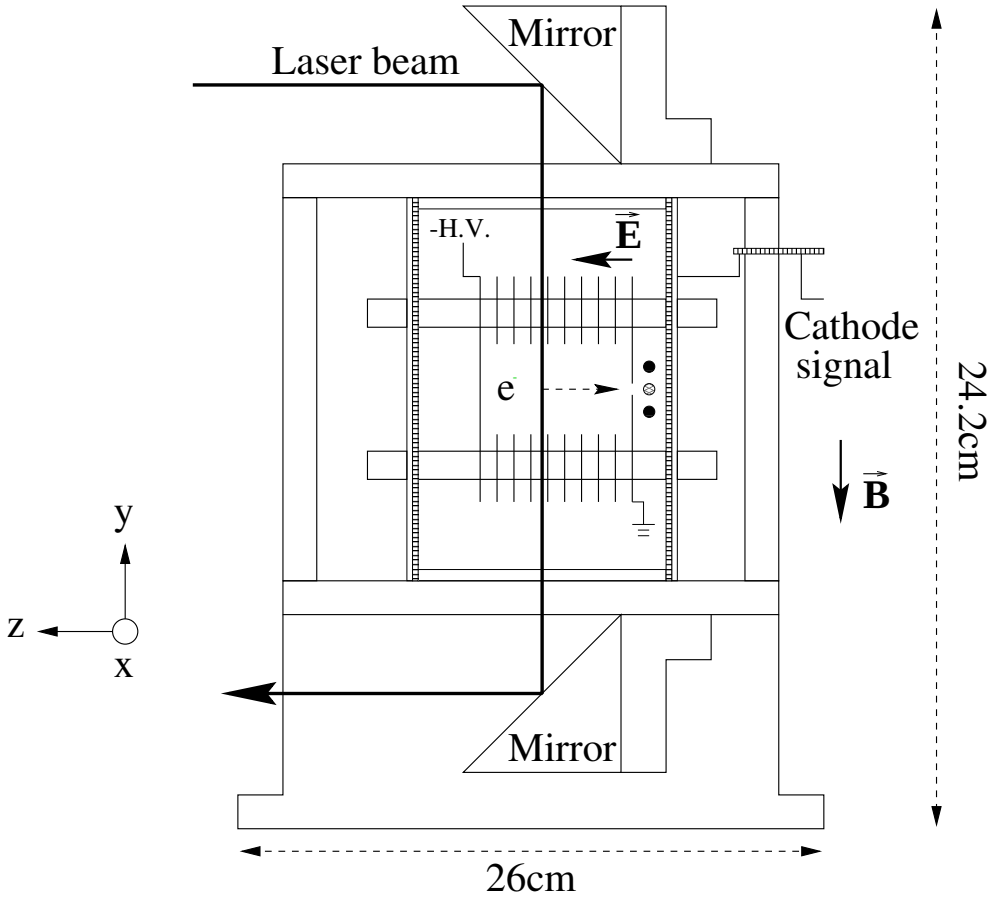

Figure 4.3: A sectioned drawing of test chamber (x-view)

plate which divides the Drift part from the Gain part has a 1×150 cm^2 slit window, and its potential was kept at the ground.

The Gain part has 3 wires. They are arranged along the y-axis, and located 5 mm behind the grounded copper plate. Two wires are the field wire (diameter 120 μm, material Au-Mo, tension 300 gW) which is connected ground in order to regulate the electric-field. The center one is an anode wire (diameter 30 μm, material Au-W, tension 70 gW). When the positive high voltage is applied on the anode wire, the wire generates strong electric-field around its surface. This strong electric-field causes the electron avalanche at very close to the wire, normally, at a few wire radii. The high voltage on the anode wire is adjusted appropriate value which make anode signals $\sim$500 mV peak voltage after amplification.

The Cathode part is located 5 mm behind the 3 wires. While the Drift part and the Gain part are divided and working independently, the Cathode part and Gain part have no divider and they work together. This part consists of 27 pieces of 20×4.8 mm^2 thin pads named Cathode pads,

the same number of read-out wires, and an circuit board. The Cathode pad is shown Fig.4.4. All pads are coated with Au because Au has the high-dielectric-constant. They are printed on a circuit board with 0.2 mm gap. Read-out wires connect each pad to each channels of the pre-amp for cathode signals.

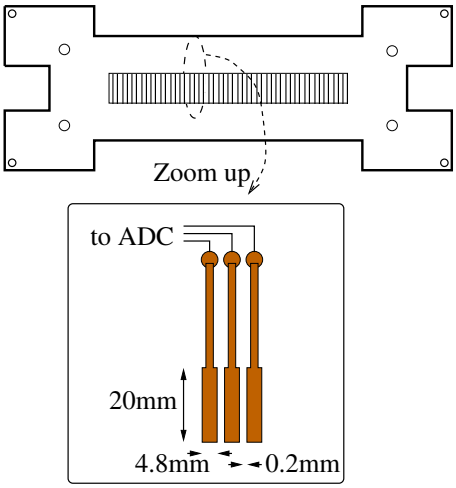

Figure 4.4: Cathode pad

4.3 Magnet

The magnetic-field is provided by an electromagnet named USHIWAKA in the KEK $\pi 2$ line. It has homogeneous field over a rectangular volume with a 54 $\times$ 64 cm^2 base area and a 30 cm gap height. The upper limit of the magnetic-field is 1.6 T. Fig.4.5 shows the induction curve of the USHIWAKA.

4.4 Data Acquisition(DAQ) System

A block diagram of the data acquisition system is shown Fig.4.6. The signal from the anode wire and cathode pads are fed into the change-integration-type pre-amp. Their outputs are led by 10 m or 30 m cables, fed into the post-amp, digitized by ADCs (Lecroy 2249W.), and read out by NEC PC98** computer. In order to measure the drift velocity simultaneously, the anode signal is divided and fed into TDC (Lecroy 2277). Trigger signal is obtained from the Q-switch of the YAG laser. Specifications for modules are shown Table.4.1.

All channels of ADCs have individual pedestal levels. The pedestal levels varies pulse by pulse due to the electric noise. In order to eliminate

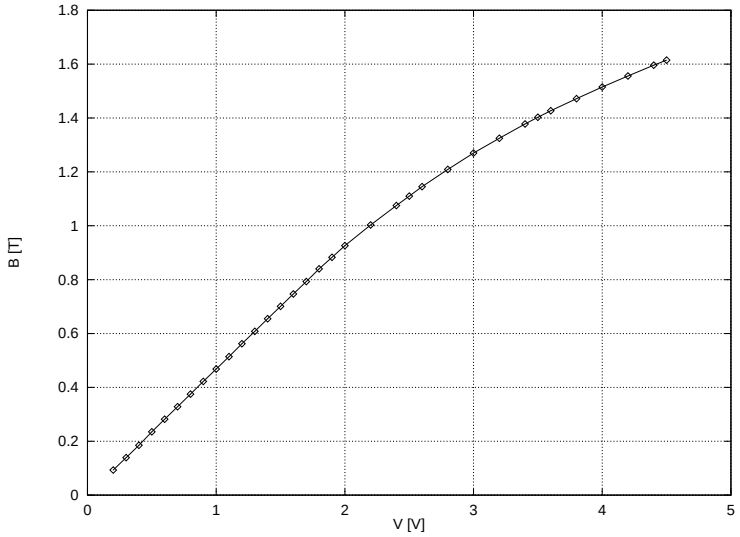

Figure 4.5: USHIWAKA V-B graph

	ADC2249W	TDC2277
No. of channel	12	32
No. of Bits	11	16
Input	Analog AC coupled $0 \sim -2.0V$	ECL
Full scale	-512pC	$65.535\mu\ sec$
Gate	Common Gate	Common start/stop
resolution	-0.25pC	1nsec/count

Table 4.1: Specifications for modules

this dispersion, an averaged value of each pad for 1000 events is subtracted from the ADC value measured for the signal.

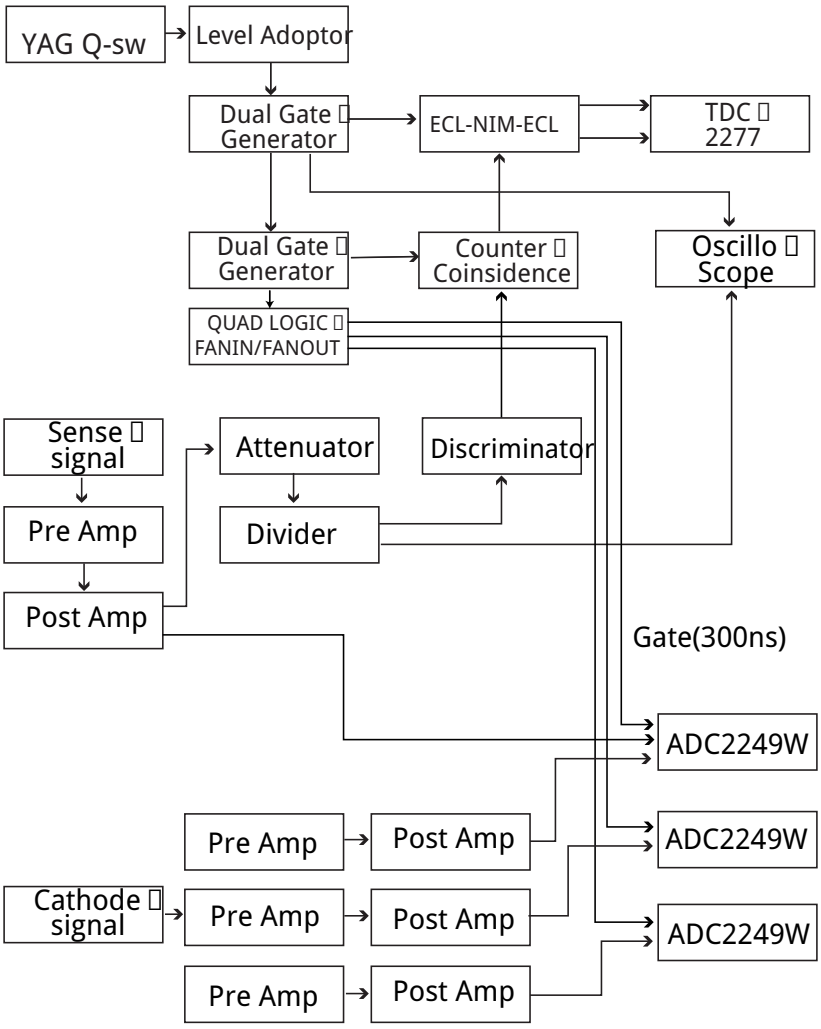

Figure 4.6: DAQ Block Diagram

Chapter 5

Experimental Procedure and Data Analysis

5.1 Experimental Procedure

The principle of the Lorentz angle measurement is illustrated in Fig.5.1. The test chamber is located at the center of the magnet with the magnetic-field in the y direction. The anode wire is placed along the x-axis, orthogonal to the magnetic-field. The laser beam which is reflected by the upper mirror incidents between copper plates, and causes ionization at the center of the copper plate windows. Owing to the homogeneous electric-field by copper plates, primary electrons drift toward anode wire, and its path is deflected along the x-axis by the magnetic-field. When those primary electrons reach a few radii of anode wire, the electron multiplication process begins and a typical drop-like avalanche covers the small location of anode wire, which induces charges on the cathode pads simultaneously. Then, those charges on cathode pads go through the read wire, of which signal is fed into the pre-amp.

In order to eliminate the influence of the electric-field disturbance near the anode wire, the deflection of drift path along x-axis is detected by taking the lest of two measurement-points which have different drift distance. Lorentz angle α is obtained as following;

$$tan\alpha = \frac{G_{z_2} - G_{z_1}}{z_2 - z_1} \tag{5.1.1}$$

where z_1 and z_2 are the laser beam position, G_{z_1} and G_{z_2} are the arrival points of drift electrons along the x-axis.

At the measurement, we carried out data taking in the following order:

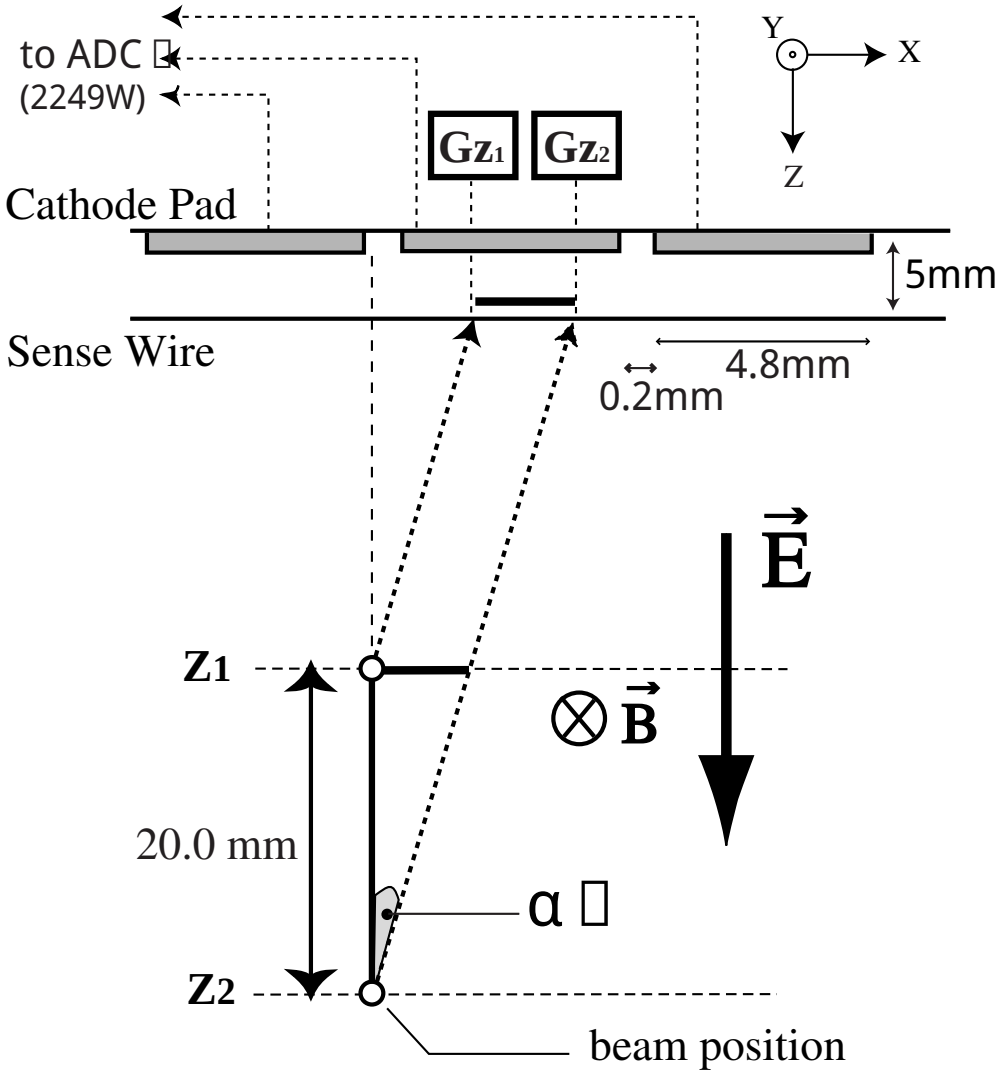

$$\tan\alpha = (Gz_2 - Gz_1) / 20.0$$

Figure 5.1: Illustration of Lorentz angle measurement

1. Choose gas mixture
2. Set the incident beam position along the x-axis, where the maximally-deflected drift electron (at 1.5 T, longest drift length) can reach within the pad No.14
3. Set magnetic-field magnitude
4. Set incident beam position along z-axis
5. Set electric-field magnitude

We changed the electric-field on the last order, because the contribution of the electric-field error to the Lorentz angle measurement is so small that the systematic error is smaller compared to other factors, for the CO_2-isobutane gas mixture.

5.2 Charge Centroid Method

The arrival point G of the cluster of the drift electrons is calculated as the weighted average of the positions of the pads carrying induced charges. We call the point G the center of gravity. This section explains of how to get the center of gravity.

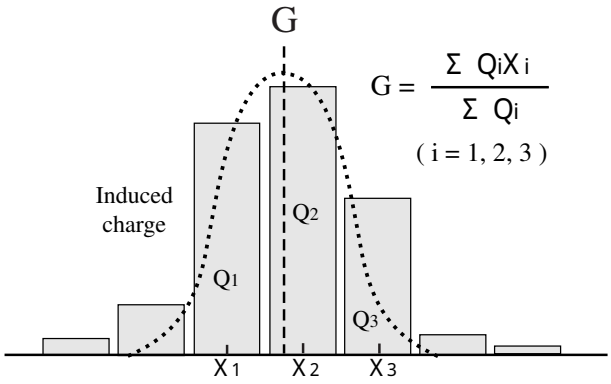

Figure 5.2: Induced charges on cathode pads

Fig.5.2 sketches a typical induced charge distribution on cathode pads, where Q_i (i = 1,2,3) is the induced charge and x_i is the center position of pad No.i. We calculated the center of gravity as follows:

1. we look for the pad having the largest amount of induced charge,
2. we checked if the adjacent pads (left and right neighbor) had induced charges above threshold (S/N=2), then

3. we calculated the center of gravity as

$$G = \frac{\sum x_i Q_i}{\sum Q_i} \tag{5.2.2}$$

using the three pads chosen in 1. and 2.

We could have chosen any add number of pads in the above calculation in principle. It is, however, necessary to limit the number in practice to avoid any measurement error due to bad signal to noise ratios on side pads.

5.3 Correction of the Induced Charges on Each Cathode Pad

When all pads are on the same condition and given same avalanche, induced charge of those pads should be same. However, in practically, there are some difference on their induced charge because of some electrical noises and so on. This problem gives an influence to center of gravity of charge strongly, therefore, each pad should be corrected by using the anode wire (avalanche) charge. The correction procedure is following;

i. Select a pad and move the laser beam position on the center of the the pad

ii. 1000 events data taking

iii. Take the ratio of the cathode charge ($d(j)$) to the anode charge ($a(j)$) for each event

iv. Take the average ratio ($D(i)$) for 1000 event

$$D(i) = \left(\sum_{j=1}^{1000} \frac{d(j)}{a(j)} \right) \times \frac{1}{1000} \tag{5.3.3}$$

v. Measure $D(i)$'s for every pad by moving the laser beam x position at an interval of 5 mm (move to the next pad center)

vi. Take the average of $D(i)$ for all 27 pads and compare with each $D(i)$

$$\overline{D(i)} \;=\; \frac{\sum_{i=1}^{27} D(i)}{27} \tag{5.3.4}$$

$$k(i) = \frac{\overline{D(i)}}{D(i)}$$
$$(i = 1, 2, ..., 27) \tag{5.3.5}$$

where $k(i)$(i=1,2,...,27) is the compensation constant of the induced charge on the individual cathode pad. The ADC count for each channel are corrected by multiplying $k(i)$.

5.4 Calibration

After the correction of the induced charge, the position G is obtained by equation 5.2.2. Owing to small gaps between two pads, and because of using 3-pad center of gravity method, the measured value of G is jumping every 5 mm also. Fig.5.3 shows a relation of the laser beam position x and the G, and line-fitted functions.

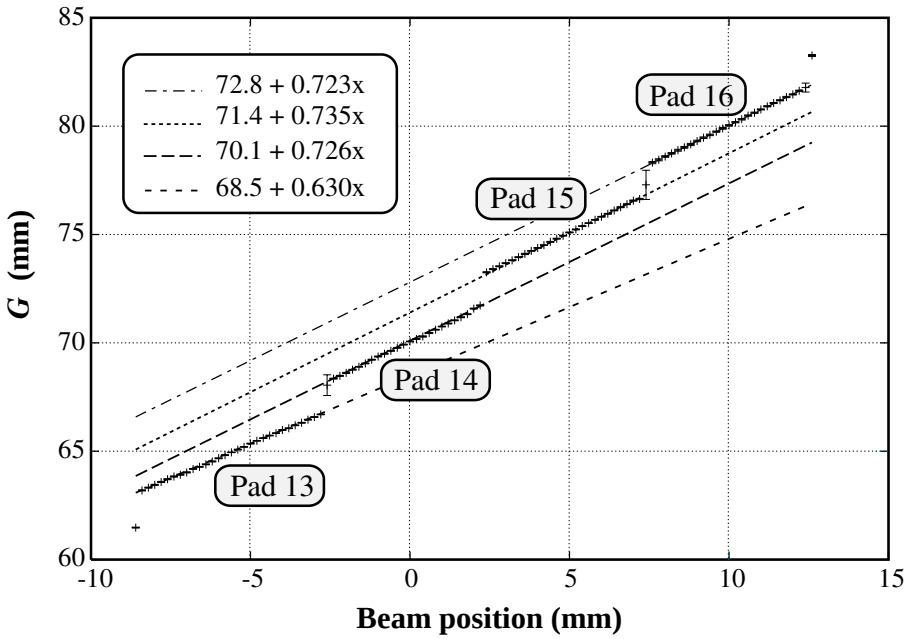

Figure 5.3: Calibration curves of center of gravity (pad 13-16)

Note the G does not correspond to the x by 1:1. It comes from using the 3-pad Center-of-Gravity Method. At the line part, mobility of G is smaller than real x coordinate. And on the gap part, mobility of G is larger than real x coordinate. For that reason, the measured value of G has to be transformed to the real position by use of the calibration curve. Fortunately, The Lorentz angle of CO_2-Isobutane is so small that drift electrons don't deflect more than

one pad distance along the x-axis, therefore, through the all experiment, all drift electrons arrive at pad No.14. We used only 3 pads, pad No. 13, 14, and 15 for the data analysis.

The position resolution obtained by 3 pads is shown in Fig.5.4. Four points at $x = 62.2$, 67.8, 73.0, and 78.4 can not be seen in the graph, because those σ are so large that get over the range of vertical axis. This phenomena occur at the gaps of two pads. In generally, the resolution at the pad gap should be better than at the center of pads – because the mobility of G is larger than real x coordinate as described above –, however, the 3-pad center of gravity Method leads opposite result. That is a problem of 3-pad center of gravity Method. It needs some improvement at the number of used pads and the weight method to get better resolution [6].

In this measurement, we did not use those pad gaps for the detection of drift electrons. The reason is to obtain all data at closely same condition. Because a pad gap is smaller than maximum deflection of G, using pad gap means using two function for compensation of G at gap part and line part respectively. The Lorentz angle of CO_2-isobutane gas mixture is so small that any small difference should gives an influence to the results.

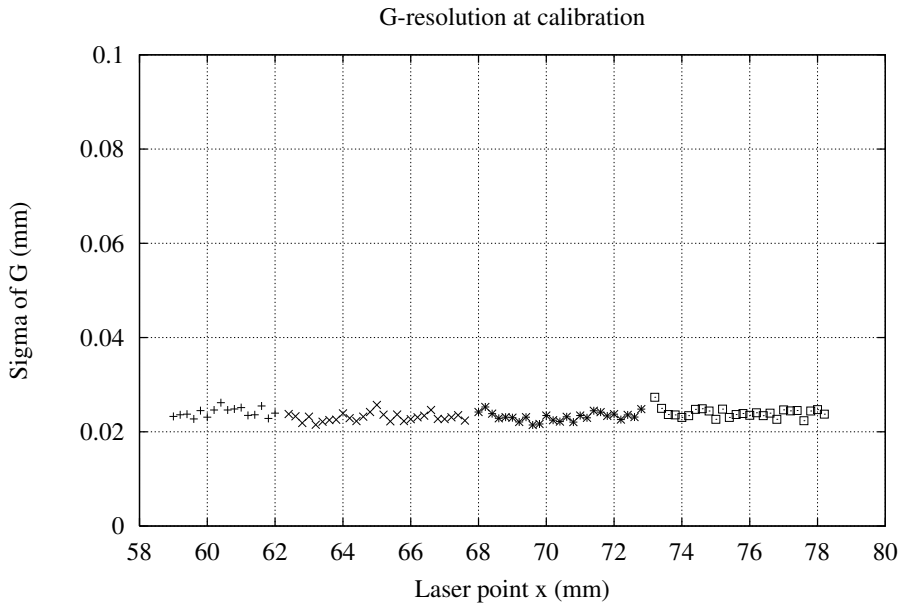

Figure 5.4: x dependence of σ (pad13-16). The σ at $x = 62.2$, 67.8, 73.0, and 78.4 are above the range of vertical axis. The resolution of G is $\sim 30\mu$m.

Chapter 6

Experimental Results

6.1 Electric-Field Dependence of the Lorentz Angle

We measured the Lorentz angle for CO_2-Isobutane mixtures, 90:10, 95:5 and 85:15, in the electric-field range between 0.2 and 2.0 kV/cm and under the magnetic-field between 0 and 1.5 T. All measurements have been done at the room temperature and at the atmospheric pressures.

Fig.6.1 shows results for the 90:10 mixture. It can be divided into two region at the electric-field of 1.4 kV/cm. In the lower electric-field, there is a plateau region at each magnetic-field. In the upper region, $\tan\alpha$ increases slightly, especially at the higher magnetic-field. Fig.6.2 and Fig.6.2 are the results for the 95:5 and 85:15 mixture, respectively, which show the same tendency with the 90:10 mixture.

The errors was estimated by the standard deviation of G. They include the contribution of the uncertainties which coming from the error on the electric and magnetic field value provided by the power supply and from small pressure and temperature fluctuations. However, especially at the higher magnetic-field, those errors are more than 10 times bigger compared to the spatial resolution of the chamber itself (see Fig.5.4). Therefore, another dominant contribution may exists. This problem is discussed in next chapter.

6.2 Extrapolation of the Lorentz Angle to 2 T

As described in the chapter 1, JLC-CDC is operated under the magnetic-field of 2.0 T. Due to the limitation of USHIWAKA-magnet, our data was taken at the highest magnet field of 1.5 T. Now, the obtained results should be

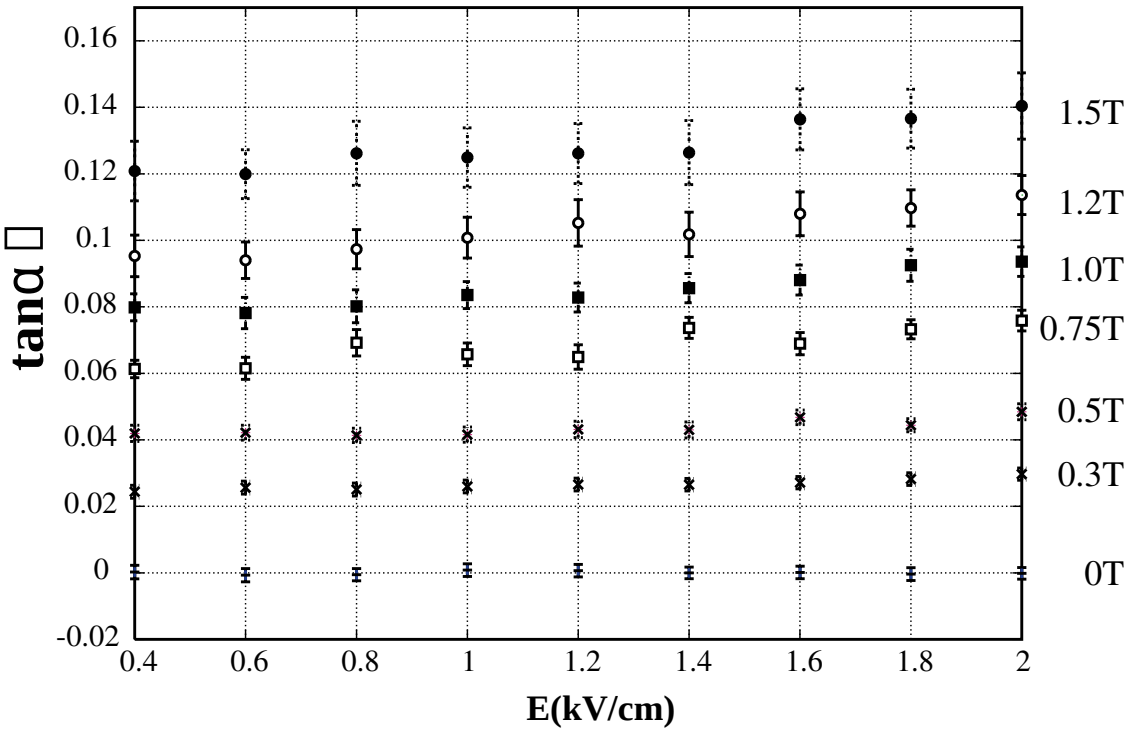

Figure 6.1: tanα for the CO_2-isobutane (90:10) mixture versus the electric-field, under the magnetic-fields B=0, 0.3, 0.5, 0.75, 1.0, 1.2, and 1.5 T.

extrapolated to 2.0 T.

The extrapolation was done by a linear fitting. Fig.6.4 shows the extrapolated value at 2 T, where the gas mixture is CO_2-isobutane (90:10) and the electric-field is 1.0 kV/cm. The electric-field of 1.0 kV/cm is a designed value of JLC-CDC at present. The extrapolation error is estimated at 5.9 %.

Another two calculations in Fig.6.5 and Fig.6.6 are for the gas mixtures (95:5) and (85:15), in which extrapolation errors are 5.7 % and 4.7 %, respectively.

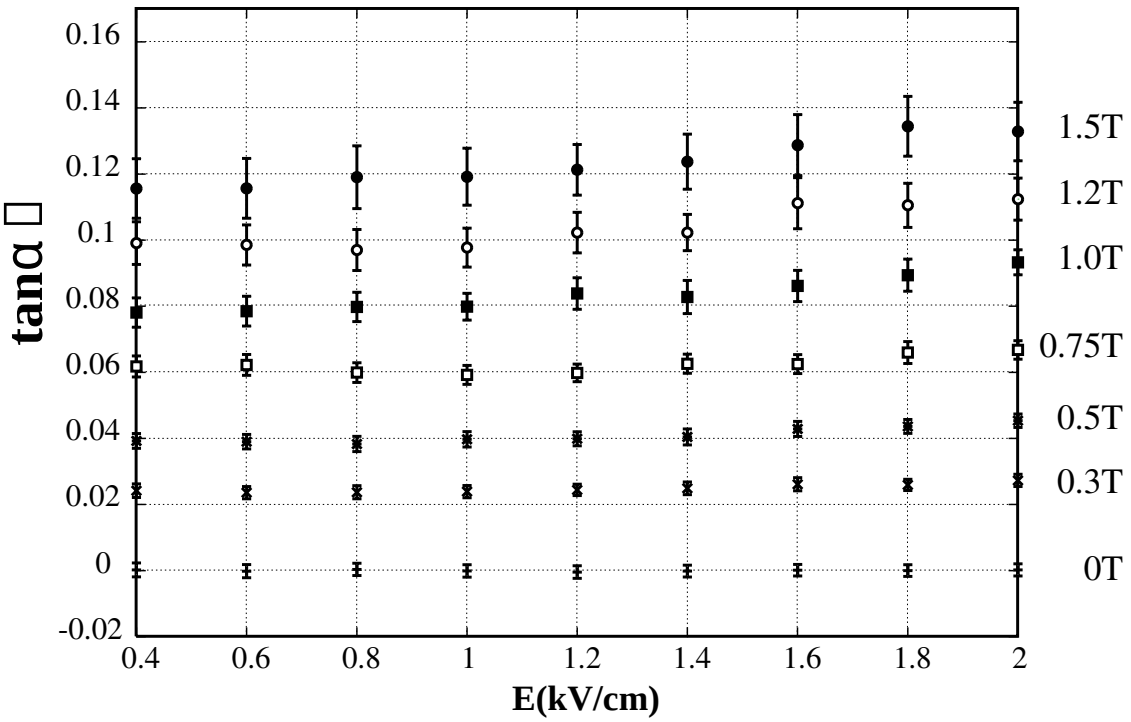

Figure 6.2: tanα of CO_2-isobutane (95:5) mixture

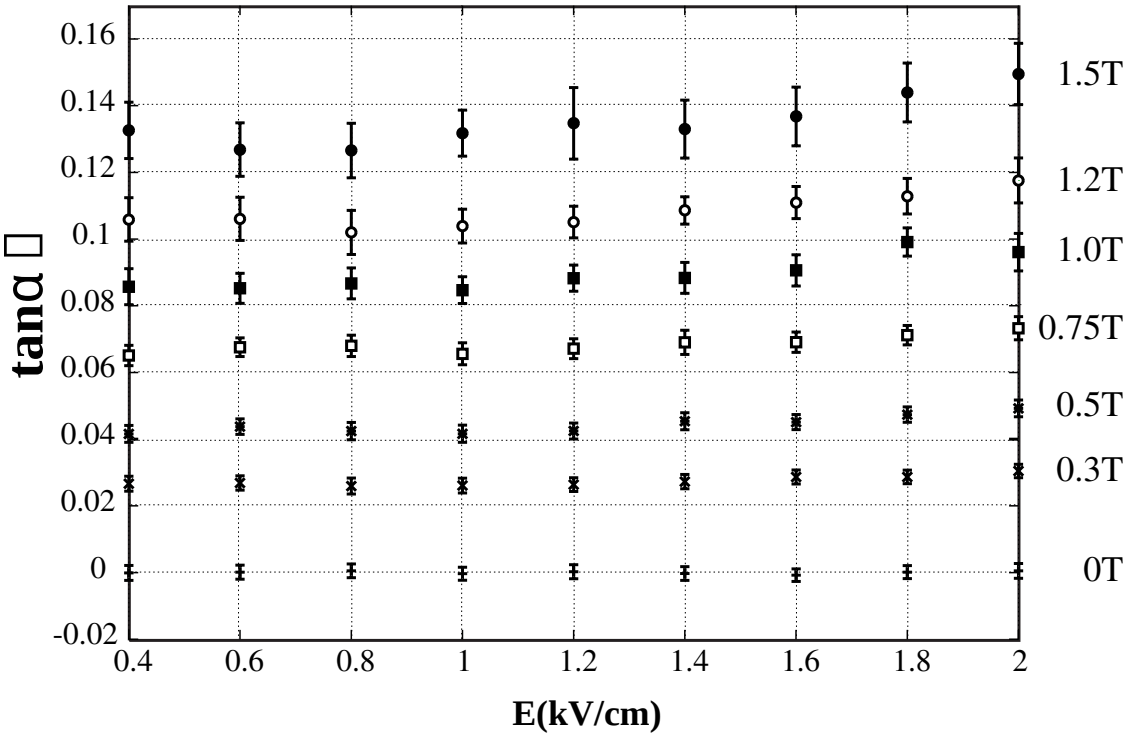

Figure 6.3: tanα of CO_2-isobutane (85:15) mixture

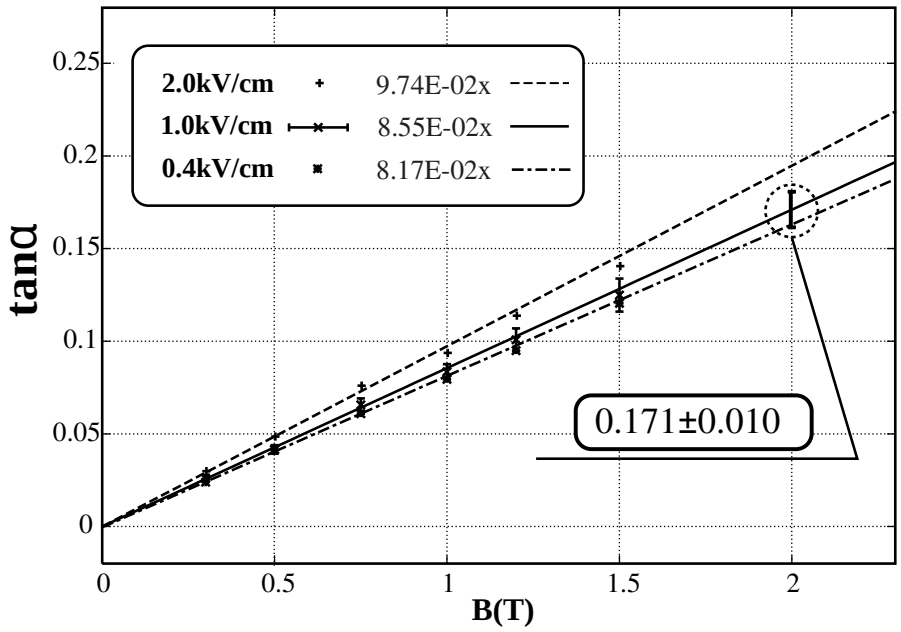

Figure 6.4: Lorentz angle extrapolated at 2.0T(90:10)

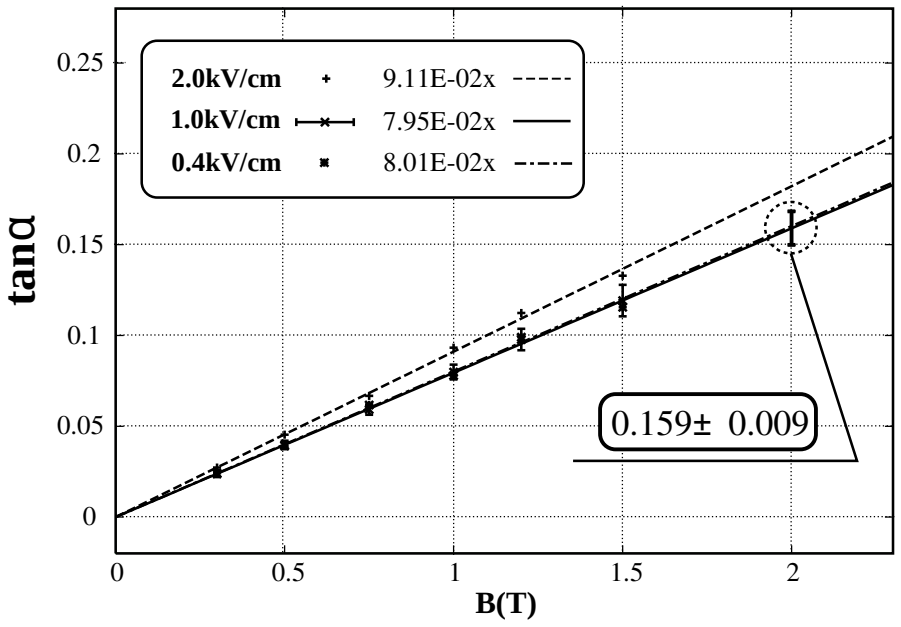

Figure 6.5: Lorentz angle extrapolated at 2.0T(95:5)

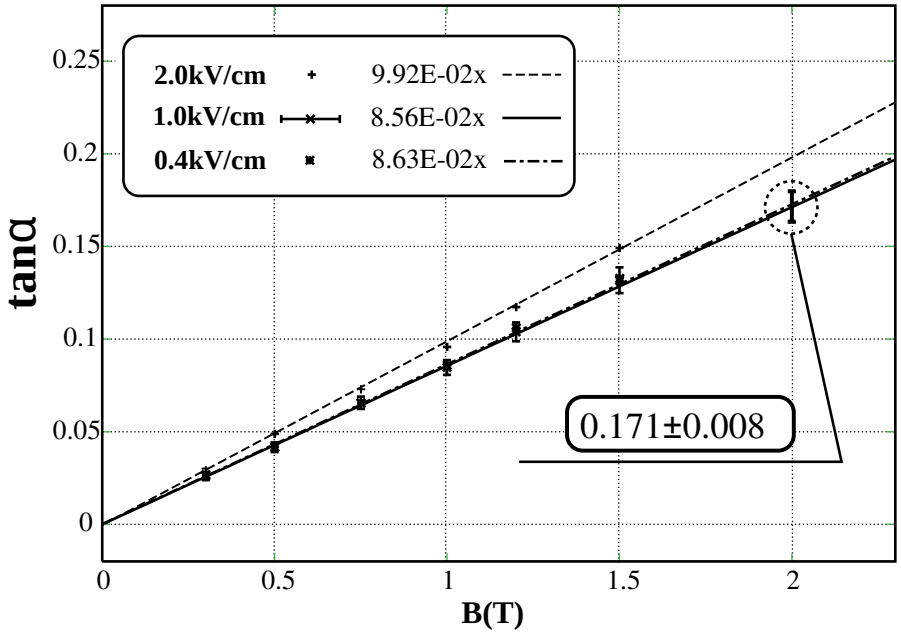

Figure 6.6: Lorentz angle extrapolated at 2.0T(85:15)

6.3 Comparison with GARFIELD Simulations

We calculated the Lorentz angle for CO_2-isobutane gas mixture by using the gaseous detectors simulation program GARFIELD. Fig.6.7 shows the results of Lorentz angle measurements for different magnetic fields as a function of electric field together with the GARFIELD simulation. In the both the simulations and the experimental data show a tendency of non-linearity at upper 1.4 kV/cm, however, the values of the $tan\alpha$ of simulations are systematically less than the experimental data. In order to explain these small disagreements, we need more detailed studies of the GARFIELD simulation program and the analysis of the experimental data.

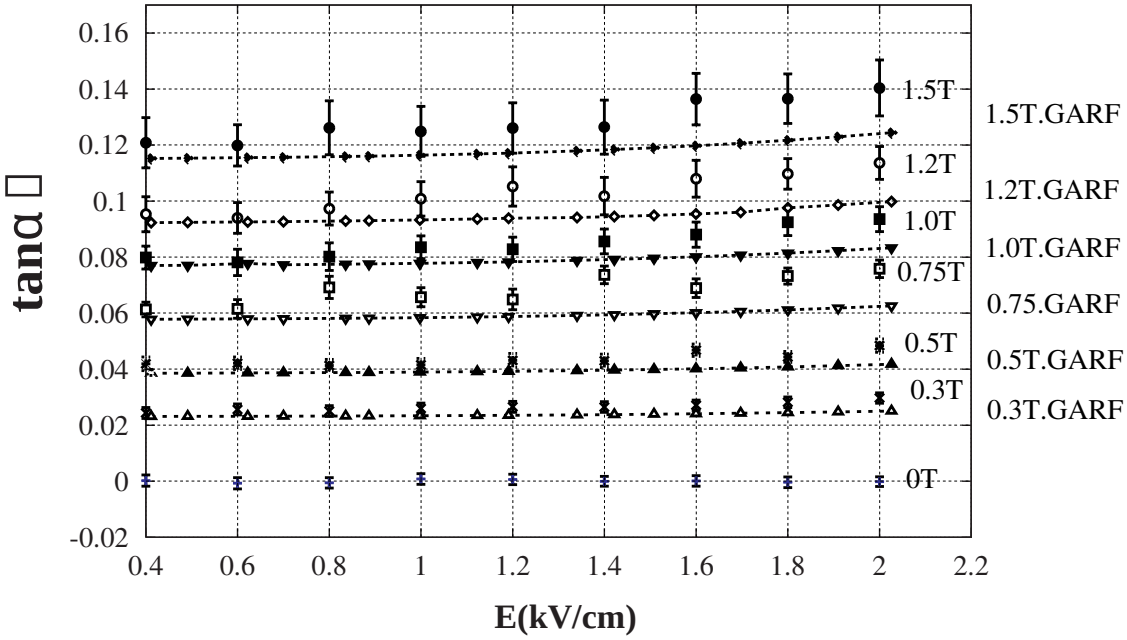

Figure 6.7: Comparison with GARFIELD simulations for the CO_2-isobutane (90:10)

6.4 Electric-Field Dependence of ψ

Electric-field dependence of $\tan\alpha$ (Fig.6.1, 6.2, and 6.3) shows a tendency of non-linearity at upper 1.4 kV/cm. In this section, we try to explain this tendency by the view of the drift velocity.

A velocity $\mathbf{v}_B$ (magnetic drift velocity) is defined as follows: [7]

$$\mathbf{v}_B \equiv \frac{\mathbf{E}}{\mathbf{B}} \tan\alpha \tag{6.4.1}$$

and in general, $\mathbf{v}_B$ is approximately equal to $\mathbf{v}_{D_0}$, which is the drift velocity at the zero magnetic-field. The relation between those velocities is following,

$$\mathbf{v}_B = \psi \mathbf{v}_D \tag{6.4.2}$$

where ψ is named as the magnetic deflection coefficient. It has an unit value when the effective collision frequency between the electrons and the molecules of gas is independent of the speed of electrons between the collisions. Then, equation 6.4.1 is written as is introduced at chapter 3 :

$$\tan\alpha = \psi \frac{\mathbf{B}}{\mathbf{E}} \mathbf{v}_D \tag{6.4.3}$$

We know that the velocity of CO_2-isobutane gas mixture is almost linear to the electric-field, so that we can expect that $\tan\alpha$ probably independent of $\mathbf{E}$ if the ψ is independent of $\mathbf{E}$. Now, let we compare the equation 6.4.3 with our experimental data.

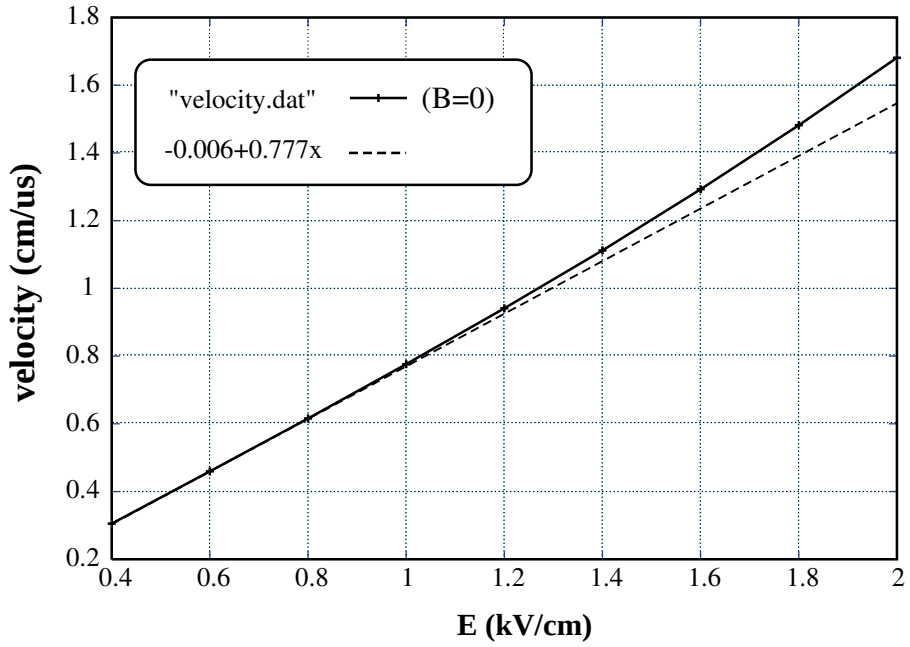

Figure 6.8: Drift velocity for the CO_2-Isobutane

Fig.6.8 is the results of our previous measurement (1996) of the drift velocity of CO_2-isobutane(90:10) as a function of electric field at the zero magnetic-field. It shows almost the same tendency as the electric-field dependence of $\tan\alpha$. At upper 1.4 kV/cm, the velocity shows the non-linear

behavior. The straight line in this figure is the line-fit to the experimental data from 0.4 to 1.0 kV/cm. According to the formula 6.4.3, the magnetic deflection coefficient ψ can be estimated as a function of electric field by using drift velocity and Lorentz angle data(see Fig.6.9).

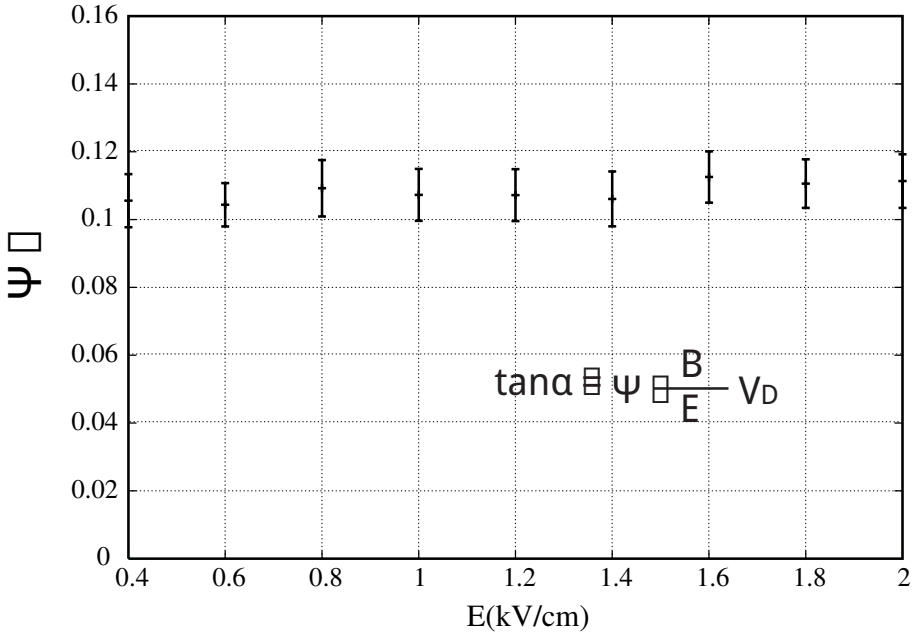

Figure 6.9: Electric-field dependence of ψ(90:10)

As we can see the ψ looks like independent of $\mathbf{E}$. That means, the effective collision frequency is independent of speed of electrons between the collisions, namely, the cross section of our gas doesn't depend on the electron's energy at our experimental condition.

Chapter 7

Discussion

Fig.6.1 implies a potential problem: the errors on tanα grows as the magnetic field increases. An analysis indicates a clue to understand the problem, which shows a variation of the center of gravity G as a function of time. Fig.7.2 shows a comparison of the time dependence of G and ADC values at 0.3 T and 1.5 T, which shows evident difference on its behavior. For all data at the high magnetic-field, G makes vibration whose amplitude depend on the magnetic field (see Fig.7.1) and its frequency is very unstable. The frequency has no correlation with the magnetic-field and the electric-field, has no reproducibility, and is much slower than 10 Hz(= data taking rate).

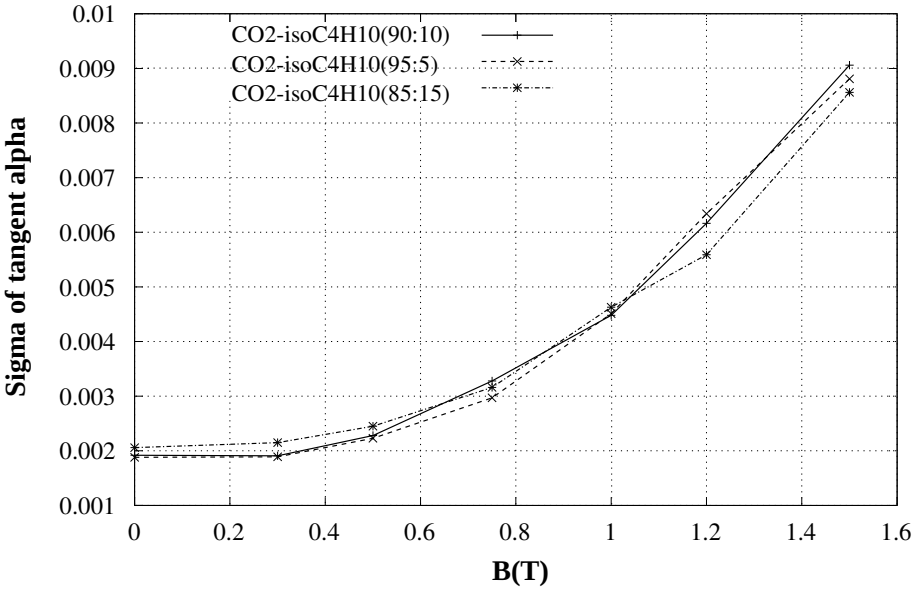

Figure 7.1: Magnetic-field dependence of σ

Right graphs of the Fig.7.2 show ADC values of 3 pads, which are normalized by the sense wire ADC at the event-by-event basis. It shows, namely, the ratio of induced charges on those of 3 pads. The value of Pad

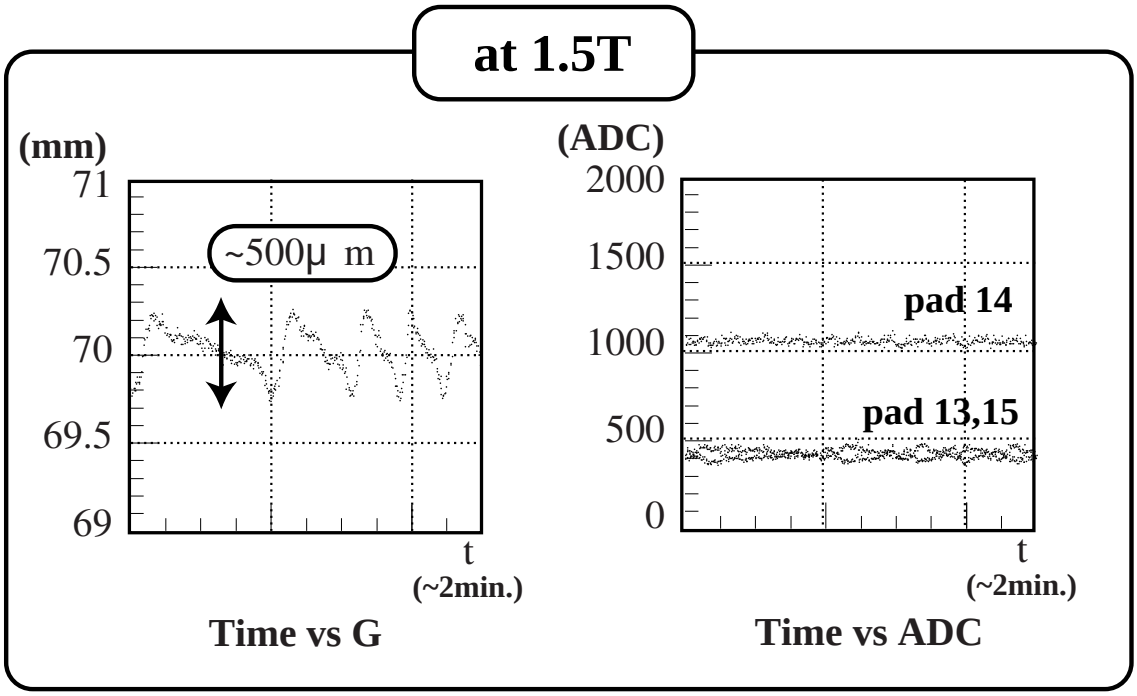

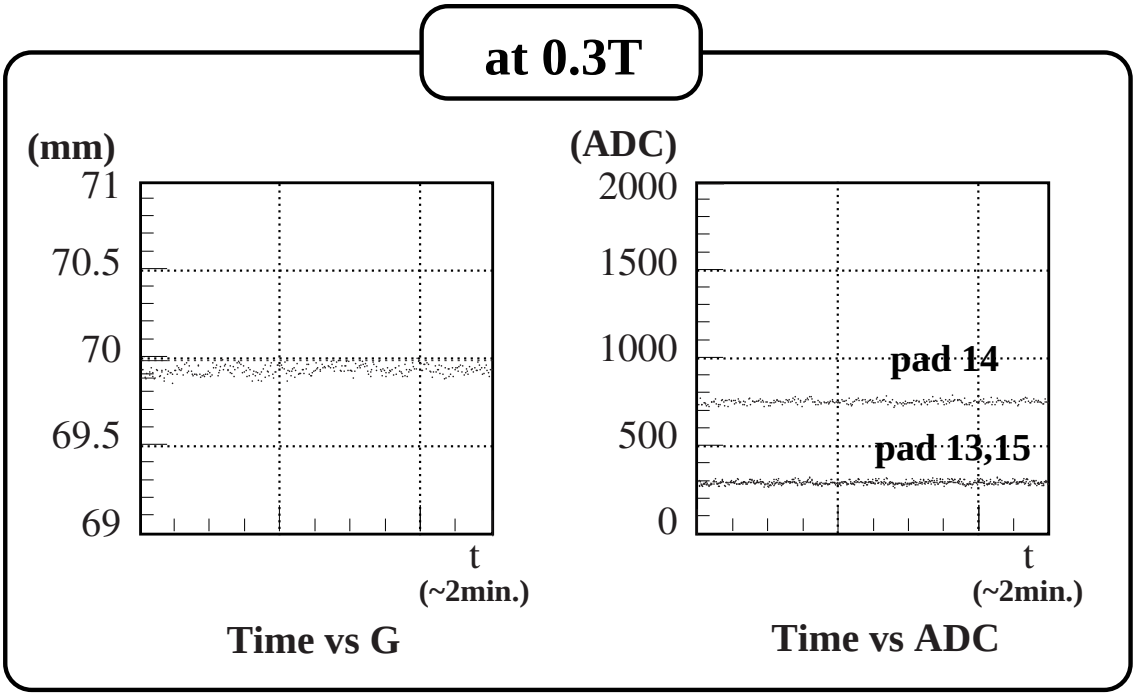

Figure 7.2: Comparison of time dependence of center of gravity at 0 T and 1.5 T

No.14 is, of course, higher than other pads because all drift electrons reach in front of this pad. Other two pad's values show curious behaviors, if one side rises up, the other side sinks down, and if one sinks down, the other rises up, with clearly the same frequency as those of the center-of gravity vibration. Those phenomena may occur when the laser point x is actually fluctuating along the x-axis. When the x moves toward pad No.15, the center of gravity G should moves same direction, then, the ADC value of the pad No.15 should increase and of the pad No.13 should decrease oppositely. When if the x moves toward the pad No.13, the inverse situation can be seen. At 1.5 T, the fluctuation increases up to 10 % by $\tan\alpha$. Although there is a relation between the fluctuation and of the magnetic-field as Fig.7.1 shows, however, it is difficult to think that the magnetic-field is fluctuating in the order of 10 %.

Another possibility is instability of the beam position. If the incident beam position fluctuates, both deflected-value of the x and drift distance may change event by event. During measurements, we observed the USHIWAKA magnet was vibrating at the high magnetic field. Although the frequency of the magnet vibration is much smaller than the frequency of G, however, some kind of beat can be produced as a result of interference among the magnet vibration and the data taking frequency, if those frequency have close value. That beet could be seen as the very slow vibration of G.

In order to study this problem and improve our measurement, we propose new experiment at the next chapter.

Chapter 8

Proposals of the Next Experiment

8.1 Two Simultaneous Parallelized Beam System

We assumed that the vibration of center of gravity G comes from the instability of the beam position. However, if a pair of center of gravity data which comes by the different drift length can be obtained simultaneously, then the values $(z_2 - z_1)$ and $(G_{z_2} - G_{z_1})$ will be stable. For example, when z_1 moves along x-axis, z_2 will moves the same direction and the same amount simultaneously, so that the fluctuation at z_1 and z_2 should cancel each other. Therefore, we propose the two simultaneous parallelized beam system for the new experiment.

Fig.8.1 is a schematic view of an optical setup. The laser beam is split into two parallel beams by using the beam splitter and led into the chamber. The ionization are induced simultaneously at the two different positions along the z-axis. The distance between two positions is 20 mm.

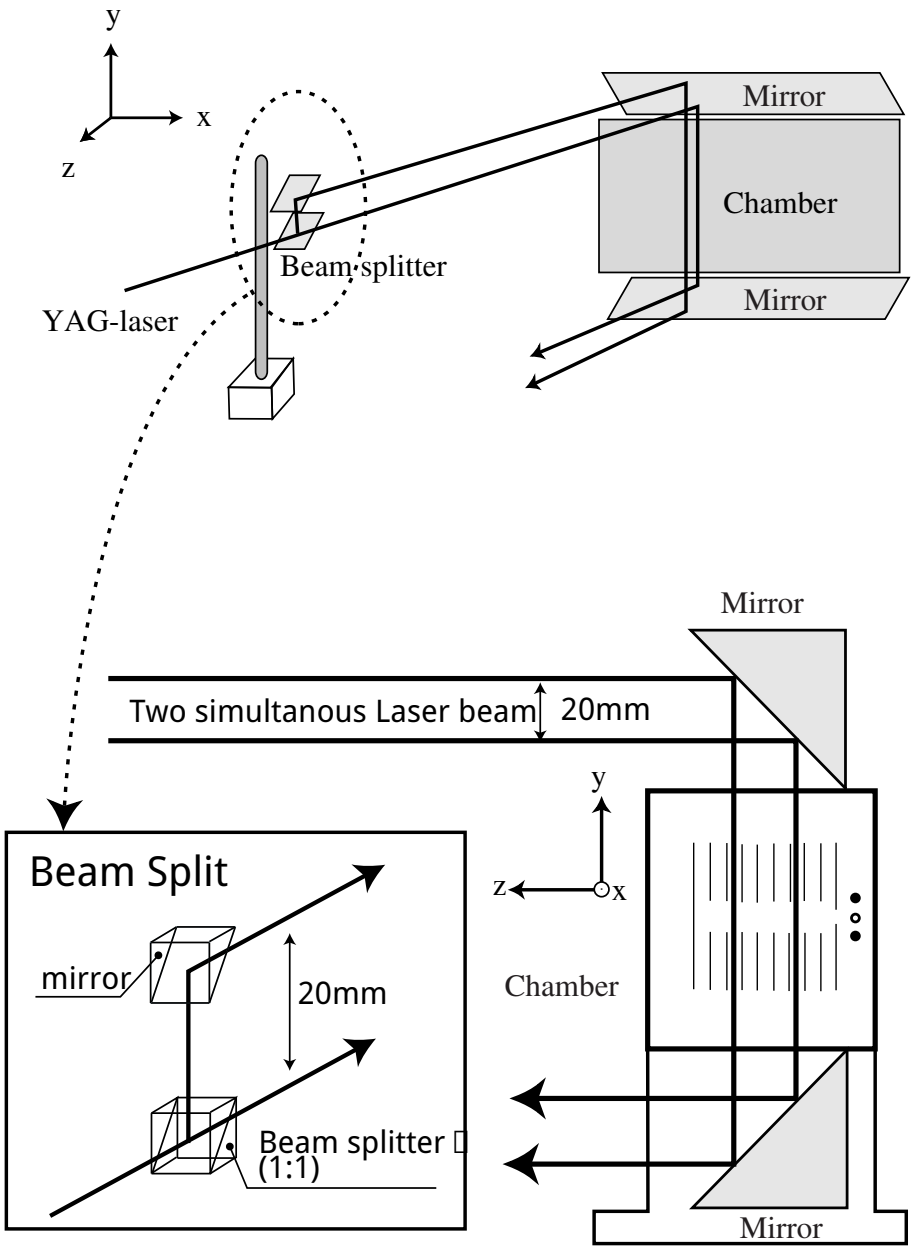

Figure 8.1: Optical setup for the new experiment using two simultaneous parallelized beam

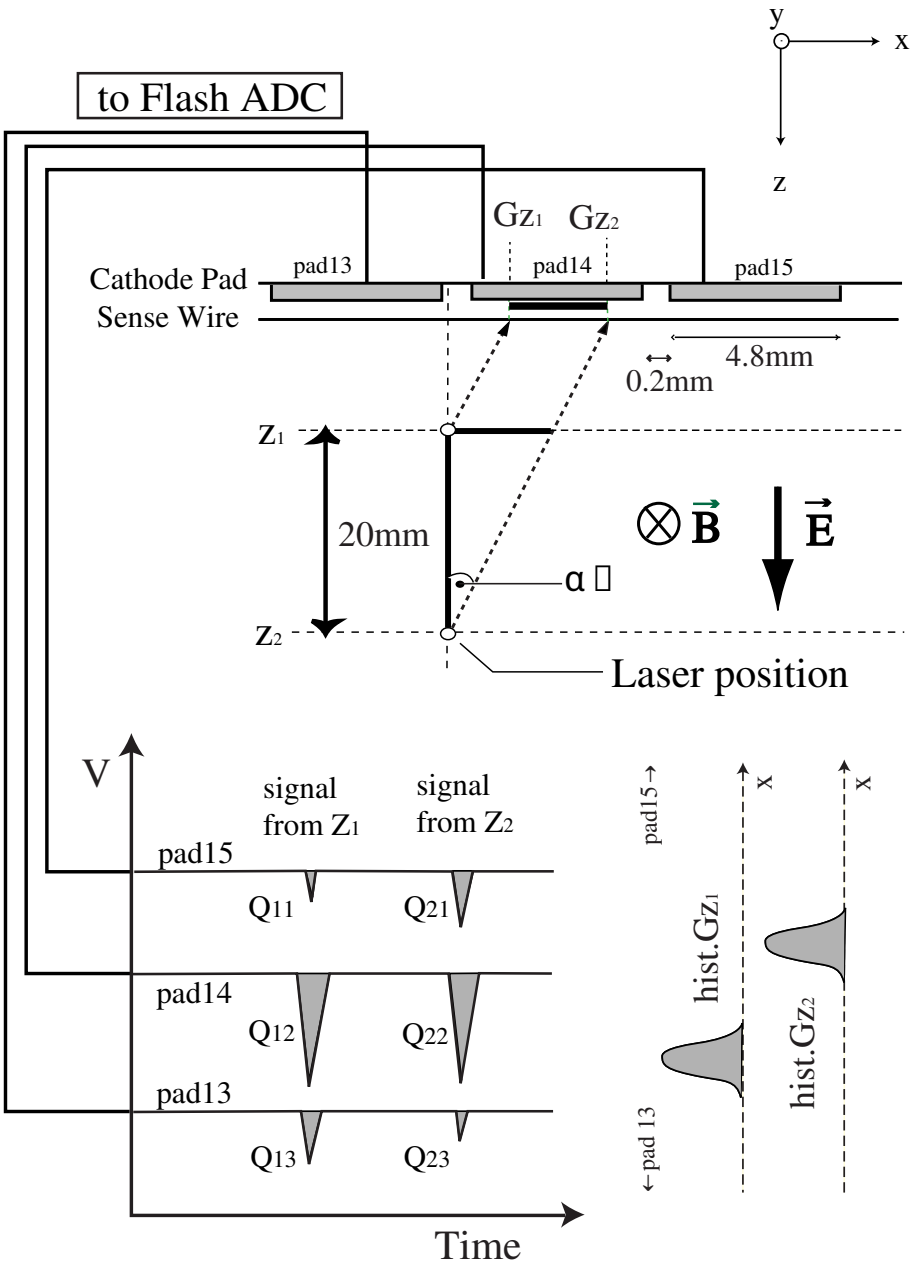

Figure 8.2: Setup of the Flash ADC

8.2 New DAQ System

Fig.8.2 shows the new Lorentz angle measurement system. It is almost same as the present measurement system except that both G_{z_1} and G_{z_2} can be obtained by one shot of laser beam. On the other hand, this improvement requires a new data acquisition system which can record two separate signals simultaneously as a single event.

In order to fulfill this requirement, we propose to use Flash ADCs. A flash ADC records the voltage of input signal at some constant sampling rate (in our case, at intervals of 2 ns). Namely, it records the pulse shape as an oscilloscope does. The induced charges on the cathode pads can then be obtained by integrating such pulse shapes. Then, the center of gravity can be calculated as before.

8.3 Calibration

Calibration data are shown in Fig.8.3, where we can see two calibration curves from two pulses. Pulse 1 and Pulse 2 represent the centers of gravity of the first and the second pulses, respectively. Both calibration curves have the same tendency, which means, the center of gravity of the both pulses are detected impartially.

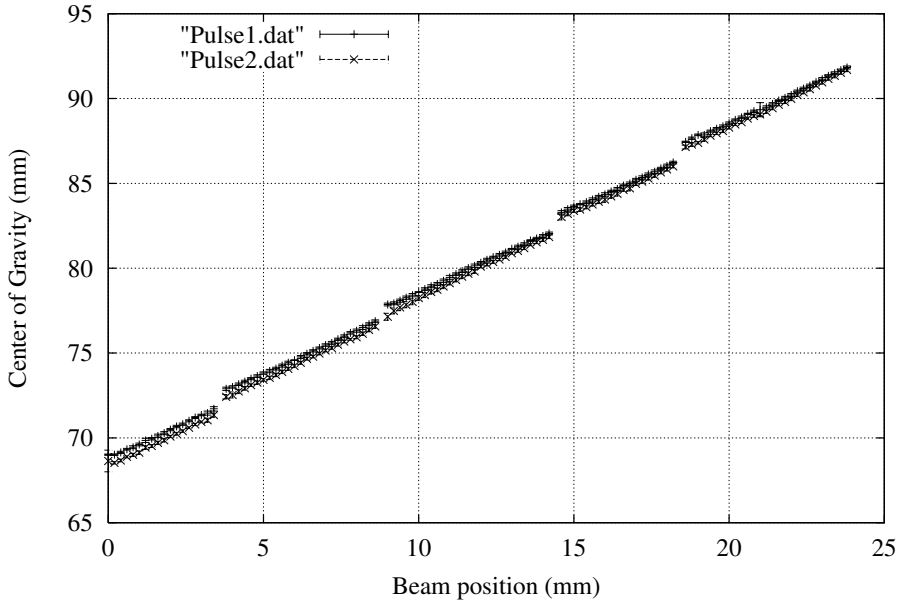

Figure 8.3: Calibration curves of center of gravity (two beams)

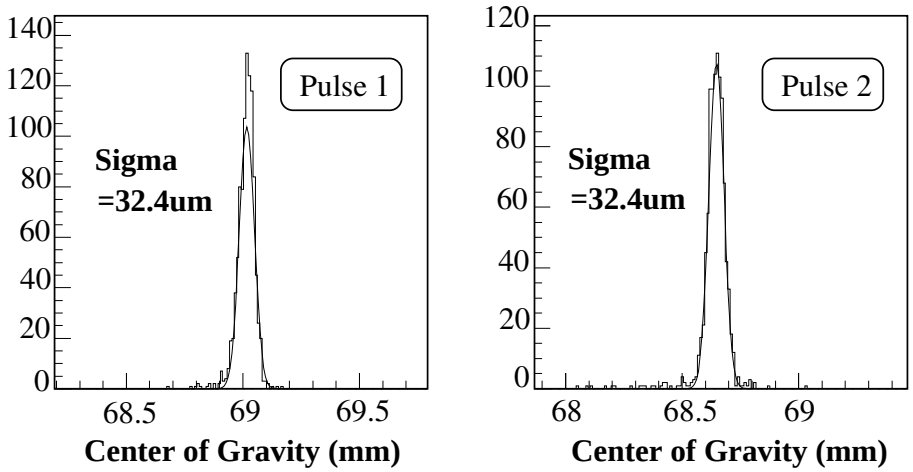

Figure 8.4: Center of gravity distributions for the 2 pulses recorded by flash ADCs.

Fig.8.4 gives histograms of the center of gravity for the both pulses corresponding to 1000 events. The position resolutions are 32.4 μm, which is consistent with the value of our previous setup (see Fig.5.4).

Chapter 9

Conclusion

We have established a Lorentz angle measurement system. Using this we measured the Lorentz angle of the CO_2-isobutane gas mixture for the different proportion (95:5), (90:10), and (85:15). The dependences of Lorentz angle versus of the electric field for different magnetic fields are shown. The extrapolated values of the Lorentz angle at the magnetic field 2.0 T are the following:

Gas mixture	$\tan\alpha$
(95:5)	0.159 ± 0.009
(90:10)	0.171 ± 0.010
(85:15)	0.171 ± 0.008

The results of the measurements of Lorentz angle are compared with the GARFIELD program. During the study we observed a small systematic disagreements between calculation. We need more detailed study of simulation program GARFIELD and more precise experimental data.

During the experiment we found the instability of the laser beam position at the higher magnetic fields which makes worse the experimental data. In order to prevent from this we propose a new Lorentz angle measurement system by using two simultaneous laser beams.

Acknowledgments

I would like to thank prof. O.Nitoh and prof. K.Takahashi, my companies of Nitoh-Lab, and the members of JLC physics working group.

I'm very grateful to my professors for their useful advices, fourth grade students for their help of calibration data taking, and H.Kuroiwa for his great helps from the beginning of this experiment.

I also specially thank N.Khalatyan who gives me many graces and advice through the all experiment and analysis. This thesis wouldn't finish without his great help. Y.Kurihara, K.Fujii, and H.Okuno helped me about the experiment and discussions, I also give my faithful thanks for their helps.

Bibliography

[1] JLC-CDC group
"JLC-I" *KEK Report 92-16 (December 1992)*

[2] JLC-CDC group
a paper on cosmic ray test, in preparation.

[3] T.Kleinknecht, (Japanese translator: K.Takahashi,H.Yoshiki)
"DETEKTREN FUR̈ TEILCHENSTRAHLUNG"
B.G.Teubner. Stuttgart(1984), Baifukan(Japanese version)(1987)

[4] T.Kunst,B.Götz,B.Schmidt
"Precision measurements of magnetic deflection angle and drift velocities in crossed electric and magnetic-fields"
Nucl. Instr. and Meth. **A324***(1993)127-140*

[5] N.Okazaki
"Lorentz angle measurements of drift electrons in crossed electric and magnetic field with a UV Laser"
Master thesis in TUAT,(1999)

[6] K.Lau,B.Mayes,J.Pyrlik
"Test results of a high precision cathode strip chamber based on plastic streamer tubes"
Nucl. Instr. and Meth. **A354***(1995)376-388*

[7] L.G.H.Huxley and R.W.Crompton
"The Diffusion and Drift of Electrons in Gases"
Wiley, New York (1974) chap.8.2.2

[8] K.Yagi
"Measurements of magnetic deflection angle in crossed electric and magnetic field"
Master thesis in TUAT,(1997)